Journal of Crystal Growth 464 (2017) 94–99

Contents lists available at ScienceDirect

Journal of Crystal Growth

journal homepage: www.elsevier.com/locate/jcrysgro

Electroluminescence-based quality characterization of quantum wells for solar cell applications

Kasidit Toprasertpong[a,*], Tomoyuki Inoue[a], Amaury Delamarre[a,b], Kentaroh Watanabe[a,b], Jean-François Guillemoles[b,c], Masakazu Sugiyama[a,b], Yoshiaki Nakano[a,b]

[a] School of Engineering, the University of Tokyo, 2-11-16 Yayoi, Bunkyo-ku, Tokyo 113-0032, Japan
[b] NextPV LIA CNRS-RCAST, the University of Tokyo, 4-6-1 Komaba, Meguro-ku, Tokyo 153-8904, Japan
[c] Institute for Research and Development on Photovoltaic Energy (IRDEP), 6 Quai Watier, 78401 Chatou, France

ARTICLE INFO

Keywords:
A1. Characterization
A3. Quantum wells
B1. Nanomaterials
B2. Semiconducting III-V materials
B3. Solar cells

ABSTRACT

Material quality is a critical factor which determines the performance, particularly the open-circuit voltage, of multiple quantum well (MQW) solar cells. In this study, we report an electroluminescence-based characterization technique for evaluating luminescence efficiency and Shockley-Read-Hall recombination lifetime in MQW structures as a measure of the material quality. As a demonstration, various structures of InGaAs/GaAsP MQWs inserted in GaAs solar cells are investigated. The complete compensation of strain and the insertion of GaAs interlayers between heterointerfaces result in significant improvement of electroluminescence homogeneity, external luminescence efficiency, and lifetime, agreeing well with the tendency of the open-circuit voltage. We show that this characterization technique can detect even subtle degradations, which are not easily detectable by other typical techniques, such as in-situ reflection, X-ray diffraction, and spectral and transient photoluminescence, but still have a significant impact on the performance of solar cells.

1. Introduction

III-V multi-junction solar cells are the dominant technology in the space application and offer a potential approach to reduce the electricity generation cost of terrestrial solar cells, owing to increased conversion efficiency [1]. With the use of materials with different bandgaps, multi-junction solar cells today are the most efficient solar cell technology with energy conversion efficiencies above 40% at submodule level [2]. Nevertheless, their efficiencies are still much lower than the theoretical value [3] and leave large room for improvement. One main issue which hinders the efficiency improvement is a lack of high quality materials with optimal bandgaps while being lattice-matched with the underlying substrate. The requirement of lattice-matched materials with optimal bandgaps becomes more severe in solar cells with a larger number of junctions.

Strain-balanced multiple quantum well (MQW) structures have been proposed as promising materials to realize the optimal bandgap combination [4]. They consist of compressively-strained *wells* whose absorption profile can be engineered, and tensile-strained *barriers* which compensate the strain before the well layers reach the critical thickness. By alternately stacking wells and barriers, a structure with the designed effective bandgap can be achieved with zero net strain, thus effectively lattice-matched. In this way, strain-balanced MQWs expand the possible bandgap range for lattice-matched materials. Various III-V alloy materials have been explored [5–10], and there is a report that MQWs improve the efficiency compared to the standard multi-junction solar cells [11].

Similarly to other solar cells, material quality is a critical parameter that affects the performance of MQW solar cells. In addition to the quality of each layer, MQWs may suffer from quality issues related to their large number of heterointerfaces. In strain-balanced material systems, strain in each layer or imperfect strain-balancing condition can be possible factors that degrade the quality. Therefore, an appropriate characterization technique for evaluating the quality of MQWs is important for systematic improvement of growth condition, structure design, and hence device performance.

Electroluminescence (EL) is a well-known technique for characterizing material properties. EL intensity is directly related to the material quality, and the concept of external and internal luminescence efficiency, parameters indicating how close the cell is to the radiative limit, has recently been used for more quantitative analysis of EL [12–14]. EL has been used to evaluate a wide range of solar cells including silicon, III-V, Cu(InGa)Se_2, organic, and multi-junction solar cells [13–18]. In this paper, we introduce this EL technique to evaluate the

* Corresponding author.
E-mail address: toprasertpong@hotaka.t.u-tokyo.ac.jp (K. Toprasertpong).

http://dx.doi.org/10.1016/j.jcrysgro.2016.10.056

Available online 26 October 2016

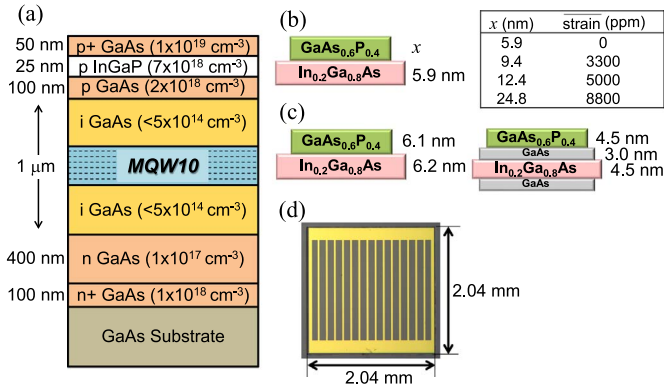

Fig. 1. Schematic of (a) cell structure containing 10-period MQW (not to scale), (b) MQWs with different barrier thicknesses. The right table shows the barrier thickness and averaged strain. (c) MQWs without and with GaAs interlayers. (d) Cell picture with front electrode.

luminescence efficiency, non-radiative recombination lifetime, and consequently the quality of MQW structures. InGaAs(well)/GaAsP(barrier) MQWs with different strain accumulations and different heterointerface treatments is investigated using EL as well as other characterization techniques, and the comparison among the techniques is discussed.

2. Methods and experimental procedure

2.1. Sample preparation

MQW solar cells in this study were grown in a horizontal metal-organic vapor phase epitaxy reactor (AIX 200/4, AIXTRON) on (001) n-doped GaAs substrates under the pressure of 10 kPa and the temperature of 610 °C. Trimethylgallium, trimethylindium, tertiarybutylarsine, and tertiarybutylphosphine were used as main precursors and dimethylzinc and hydrogen sulfide were used as doping precursors with H_2 carrier gas. The cell structure is shown in Fig. 1(a). In the i-region, the unintentional background p-type doping was compensated by a proper amount of hydrogen sulfide [19] so that the net carrier concentration became below 5×10^{14} cm^{-3}.

Two sets of 10-stack $In_{0.2}Ga_{0.8}As/GaAs_{0.6}P_{0.4}$ MQW structures were employed. All MQW structures were confirmed by X-ray diffraction measurement (XRD). As shown in Fig. 1(b), the first set consisted of $In_{0.2}Ga_{0.8}As$ with the fixed thickness of 5.9 nm and $GaAs_{0.6}P_{0.4}$ with the thickness of 5.9, 9.4, 12.4 or 24.8 nm. The MQW with 5.9-nm $GaAs_{0.6}P_{0.4}$ was strain-balanced and the remaining MQWs had averaged tensile strains of 3300, 5000, 8800 ppm, respectively. All MQWs had the effective bandgap of 1.283 ± 0.001 eV as confirmed by EL and photoluminescence (PL) peaks at room temperature. The degradation from imperfect strain balancing has been reported [20] and is a straightforward demonstration of the EL technique.

As shown in Fig. 1(c), the second set contained two strain-balanced MQW structures without and with GaAs interlayers inserted in between wells and barriers: $In_{0.2}Ga_{0.8}As$(6.1 nm)/$GaAs_{0.6}P_{0.4}$(6.2 nm) MQW and $In_{0.2}Ga_{0.8}As$(4.5 nm)/GaAs(3.0 nm)/$GaAs_{0.6}P_{0.4}$(4.5 nm)/GaAs(3.0 nm) MQW. The thicknesses of wells and barriers were adjusted so that the effective bandgaps became close, 1.273 and 1.276 eV for MQWs without and with interlayers, respectively. It has been reported that the insertion of GaAs interlayers improves the crystal quality and helps increase the number of quantum-well stacks before the lattice relaxation occurs [21]. We applied the EL technique to investigate this quality improvement in a more quantitative manner.

The size of mesa-etched cells was 2.04×2.04 mm^2 with Ag(5 nm)/Au(400 nm) front ohmic electrode, leaving the cell aperture area of 2.53 mm^2 as shown in Fig. 1(d). No anti-reflection coating was applied. In addition to 10-stack MQW solar cells, we grew 20-stack MQW test samples with the same structures shown in Fig. 1(b)-(c) to obtain more comprehensive in-situ reflectance data, which will be mentioned in Section 3.3.

2.2. Electroluminescence measurement

The photon flux per unit energy per unit solid angle ϕ_{EL} emitted from a flat surface and observed as EL is given by the generalized Kirchhoff's law [22,23]

$$\phi_{EL}(E, \Delta\mu, \theta) = A(E, \theta)\frac{2\cos\theta E^2}{h^3c^2}\frac{1}{\exp[(E-\Delta\mu)/k_BT]-1}, \quad (1)$$

where E is the photon energy, $\Delta\mu$ is the quasi-Fermi level splitting, θ is the emission angle, A is the light absorptivity at the incident angle θ, h is Planck's constant, c is the speed of light, k_B is Boltzmann's constant, T is the temperature. This equation assumes that $\Delta\mu$ has a constant value in the absorbing materials. For devices with sufficient collection efficiency of photogenerated carriers, the absorptivity can be estimated from external luminescence efficiency (EQE). Furthermore, the high refractive index of III-V materials (around 3.5) bends the incoming light to be almost perpendicular to the surface, resulting in the small variation of optical path length inside the MQW region by less than 5% and allowing us to neglect the incident angle dependence of A. In this way, the total photon flux Φ_{EL} from the device surface can be obtained by integrating ϕ_{EL} over solid angle Ω and energy E [24]:

$$\Phi_{EL}(\Delta\mu) = \int\int\phi_{EL}(E, \Delta\mu, \theta)d\Omega dE = e^{\frac{\Delta\mu}{k_BT}}\int \mathrm{EQE}(E)\frac{2\pi E^2}{h^3c^2}e^{\frac{-E}{k_BT}}dE. \quad (2)$$

In (2), the term $\exp[(E-\Delta\mu)/k_BT]$ is approximated to be much larger than 1. In this study, all MQW samples show EL intensity from GaAs, the host material, 2 orders of magnitude lower than the EL from MQW; thus we neglect the recombination originating from GaAs in the discussion thereafter.

The external luminescence efficiency or external radiative efficiency η_{ext} is defined by the ratio of the number of photons emitted from the device to the number of charge carriers injected as current, and can be expressed as

$$\eta_{ext} = q\int_S \Phi_{EL}dS/J_{inj}S = q\langle\Phi_{EL}\rangle/J_{inj}, \quad (3)$$

where q is the elementary charge, S is the surface area, J_{inj} is the injection current density, and $\langle\ \rangle$ is the average over the device area.

Samples were mounted on a Peltier temperature controller set at 25 °C to measure their EL images with a CCD camera (pco.1300, pco.). The pixel relative sensitivity of the CCD array was calibrated with a Lambertian light source diffused by an integrating sphere (IS200, Thorlab). In order to obtain the accurate values of η_{ext}, the absolute EL measurement is needed. However, such measurement requires a specially calibrated system [23,25], which is not easily available. We employed the method reported in [26] for approximately calibrating the absolute EL from a typical optical system. That is, the measured EL with arbitrary unit (Φ_{exp}) and the actual EL (Φ_{EL}) are related by the measurement constant C:

$$\Phi_{exp}(\Delta\mu) = C\Phi_{EL}(\Delta\mu). \quad (4)$$

Under low current regime where the voltage drop in the series resistance is negligible, $\Delta\mu$ can be approximated by the applied voltage V. Hence, C in (4) can be obtained by substituting $\Delta\mu = qV$ in (2) and (4). The value of C should be universal for samples which are optically similar and are measured by the same optical setup. Moreover, since this calibration method is based on the assumption of a constant $\Delta\mu$, devices with high transport properties should be used to obtain C. We found that 4 MQW samples, the first two MQWs in Fig. 1(b) and the two MQWs in Fig. 1(c), gave the same value of C.

2.3. Estimation of SRH recombination lifetime

Injected electron and hole currents eventually recombine radiatively or non-radiatively. Therefore, η_{ext} is a parameter related to the fraction of the radiative recombination and is higher in materials with lower defect density. However, η_{ext} has voltage/current dependence, and is not straightforward to be used as an evaluation parameter. The Shockley-Read-Hall (SRH) recombination lifetime τ_{SRH} can be considered as a more universal parameter.

To convert experimentally-obtained η_{ext} to τ_{SRH}, the internal luminescence efficiency η_{int}, defined by the fraction of radiative recombination in one recombination event inside MQW, has to be estimated. The radiative recombination rate per area U_{rad} can be obtained from $U_{rad} = \Phi_{EL}/P_{esc}$, where P_{esc} is the probability that photons generated inside MQW can escape out of the device's surface. The injection current density is equal to the net recombination rate: $J_{inj} = q(U_{rad} + U_{nr} - P_{reabs}U_{rad})$, where U_{nr} is the non-radiative recombination rate per area and P_{reabs} is the probability that generated photons are reabsorbed. Therefore, the averaged η_{int} becomes

$$\eta_{int} = \frac{\int U_{rad}\,dS}{\int U_{rad}\,dS + \int U_{nr}\,dS} = \frac{\langle U_{rad}\rangle}{J_{inj}/q + \langle U_{rad}P_{reabs}\rangle} = \frac{\langle \Phi_{EL}/P_{esc}\rangle}{J_{inj}/q + \langle \Phi_{EL}P_{reabs}/P_{esc}\rangle}. \quad (5)$$

U_{rad} under the metal electrode, where both Φ_{EL} and P_{esc} become zero, can be estimated with $U_{rad} = \Phi_{EL}/P_{esc}$ at the electrode edge [26]. J_{inj} and Φ_{EL} in (5) can be obtained experimentally from the EL measurement, and P_{esc} and P_{reabs} can be calculated using an optical model [27].

On the other hand, η_{int} is linked to the SRH lifetime τ_{SRH} through the following equation:

$$\eta_{int} = \frac{\int B_{MQW}np\ \ dv}{\int B_{MQW}np\ \ dv + \int np/[\tau_{SRH}(n+p)]dv}, \quad (6)$$

where B_{MQW} is the radiative recombination coefficient, n and p are the electron and hole concentrations, dv is the volume element. B_{MQW} and the current-dependent depth profile of carrier concentration ($n(z, J_{inj})$, $p(z\ J_{inj})$) can be calculated from the device simulation based on the quasi-bulk approximation [28], and, in this way, η_{int} for a given τ_{SRH} and J_{inj} in (6) can be estimated. The SRH lifetime can be determined as the value of τ_{SRH} in (6) which gives the best fit with the η_{int} - J_{inj} relation experimentally obtained on the basis of (5). Here we assume that the non-radiative recombination is dominated by the SRH process with deep defect states, and the SRH lifetime is the same for electrons and holes, considering that we cannot distinguish electron and hole lifetimes in this experiment.

3. Results and discussion

3.1. Solar cell characteristics

Fig. 2(a)-(b) shows the *J-V* characteristics under 1-sun illumination. The 8800-ppm-strain MQW has such poor quality that photogenerated carriers cannot be efficiently collected even at short-circuit condition. However, since the effective bandgap was designed to be almost the same within each set, most cells show similar values of short-circuit current density J_{sc} of 21 mA/cm^2. On the other hand, they show remarkably different open-circuit voltage V_{oc}. MQWs with different strains show V_{oc} of 0.910, 0.901, 0.877, and 0.729 V, respectively in the order of increasing strain. V_{oc} of MQWs without and with interlayers are 0.905 and 0.933 V in spite of their similar J_{sc}. Considering that the difference in V_{oc} is much larger than the variation of effective bandgap, the enhancement of V_{oc} by balancing strain and inserting interlayers is attributed to the improvement of the crystal quality.

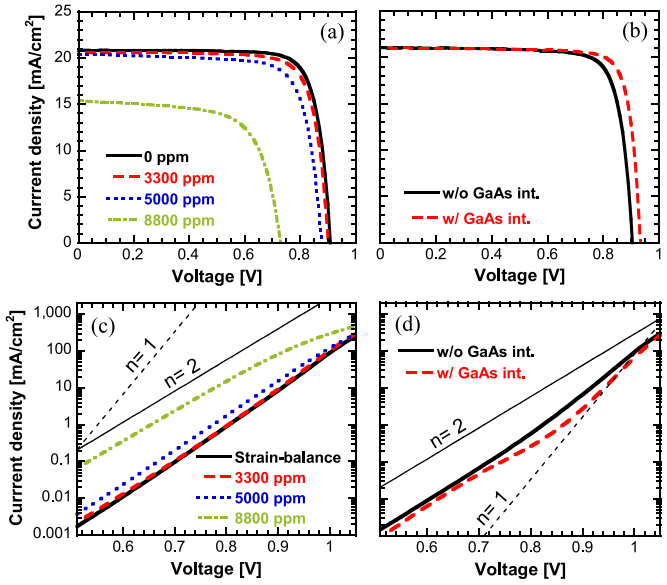

Fig. 2. *J-V* characteristics. (a) MQW cells with different net strain and (b) MQW cells without and with GaAs interlayers under 1-sun illumination. The current density under illumination was corrected by the aperture area. MQW set (c) with different net strain and (d) with and without interlayers under dark condition. Two straight lines indicate the ideality factors of 1 and 2.

This can be confirmed by the dark *J-V* characteristics shown in Fig. 2(c)-(d). MQW cells with lower V_{oc} show higher dark current with the ideality factor of 2, confirming the assumption in Section 2.3 that the non-radiative recombination component is dominated by the SRH process. MQW with GaAs interlayers has sufficiently low SRH recombination that the radiative component with the ideality factor of 1 could be clearly observed. In the next sub-section, we applied the EL measurement to confirm the above finding and to investigate the quality in a quantitative manner.

3.2. Characterization using electroluminescence

Fig. 3 shows the EL images at 0.9 V for the MQW structures with different strain accumulation. The strain-balanced MQW was found to

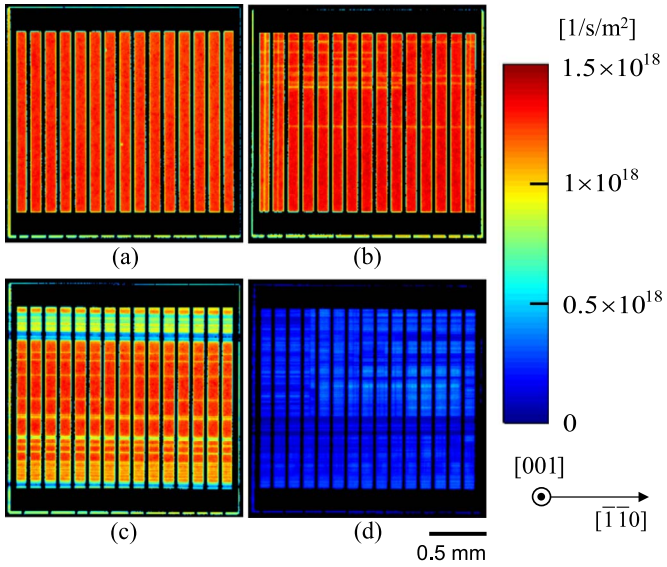

Fig. 3. EL images of MQWs with (a) 0-ppm, (b) 3300-ppm, (c) 5000-ppm, and (d) 8800-ppm strain at 0.9 V. The absolute photon flux indicated in the color bar was calibrated using (4). The dark part surrounding each cell is the etched-off region. The dark pattern inside the cells corresponds to the metal electrode.

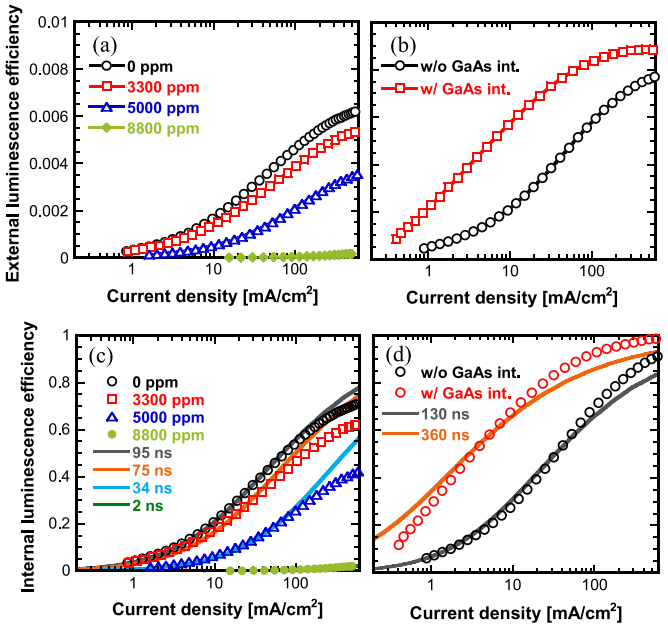

Fig. 4. External luminescence efficiency of (a) MQW cells with different net strain and (b) MQW cells without and with GaAs interlayers. Internal luminescence efficiency of MQW set (c) with different net strain and (d) with and without interlayers calculated using (5). The solid lines show the internal luminescence efficiency simulated by (6) with different SRH lifetimes.

emit the uniform luminescence. By contrast, MQWs with non-zero net strain show regions with relatively low luminescence corresponding to defects, and this becomes more prominent in MQWs with larger strain. The EL images provide the information on how defects are distributed: the defects generated from tensile-strained InGaAs/GaAsP MQWs prefer to align in the $[\bar{1}\bar{1}0]$ direction. The EL images of MQWs with and without GaAs interlayers were confirmed to be uniform without any observable defects.

The external luminescence efficiency η_{ext} of each sample under a wide range of injection current density is shown in Fig. 4(a)-(b). It is obvious from the figure that MQWs with unbalanced strain have lower η_{ext} than the strain balanced one, by a factor of approximately 2 for 5000-ppm strain and 200 for 8800-ppm strain. In addition, the insertion of GaAs interlayers was found to improve the quality significantly, agreeing well with the remarkable V_{oc} enhancement.

Fig. 4(c)-(d) shows the internal luminescence efficiency η_{int} and the fitted SRH lifetime τ_{SRH}. τ_{SRH} was estimated using the method in Section 2.3 to be 95, 75, 34, and as low as 2 ns for the MQWs with 0-, 3300-, 5000-, and 8800-ppm tensile strain, and to be 130 ns and 360 ns for the MQWs without and with GaAs interlayers, respectively. The discrepancy of the fitting curves possibly comes from our assumption made in the simulation of η_{int} by (6) that electrons and holes have the same lifetime and the injection current density is uniform over the cell area. At high injection level, the EL intensity becomes high near the metal electrode, implying that the series resistance causes lateral voltage drop at high J_{inj} and the current distribution becomes non-uniform. The tendency of τ_{SRH} observed here *quantitatively* demonstrates the effectiveness of the strain-balancing technique and the heterointerface treatment using GaAs interlayers. The origin of this prominent improvement of η_{int} to close to unity and τ_{SRH} by 3 times after the GaAs interlayer insertion has to be further investigated; it is possibly related to the reduction of the strain gradient at the interface [21] and the suppression of phosphorus carry over from GaAsP layers into InGaAs layers [29].

It is worth noting that τ_{SRH} =130 ns of the MQW without interlayers agrees well with τ_{SRH} estimated from the voltage-dependent photocurrent component in the similar MQW structure, reported in [28] that τ_{SRH} =170 ns. The agreement between τ_{SRH} estimated from injection current component (EL measurement) and photocurrent component, which are estimated with independent measurements, confirms the accuracy of obtained SRH lifetime.

3.3. Comparison with other techniques

In this section, we characterized MQWs with other typical methods for comparison. Fig. 5 shows in-situ reflectance of the 20-stack MQW test samples using 443-nm-wavelength linearly polarized light. Since substrates were rotated during the growth, DC reflectance and reflectance anisotropy (RA) are given by $\frac{1}{2}(r_{max}+r_{min})$ and $(r_{max}-r_{min})/\frac{1}{2}(r_{max}+r_{min})$, respectively, where r_{max} and r_{min} are the maximum and minimum reflectance during one revolution. The signal was oscillating due to the periodicity of MQW structures. We found that only the 8800-ppm-strain MQW shows a clear drop of DC reflectance after the growth of the 10th stack whereas other MQWs maintain the reflectance level through the MQW growth (Fig. 5(a)). The transient RA (Fig. 5(b)), which is more sensitive to the surface morphology [21], could detect a small drop during the growth of the 5000-ppm MQW as can be observed in the zoomed-in profile (Fig. 5(c)). Furthermore, RA could detect the degradation of the 8800-ppm MQW from the early stage. This implies that RA has better sensitivity to crystal degradation than DC reflectance; however it still cannot detect the difference between the 0- and 3300-ppm MQWs, which have different τ_{SRH}. Moreover, the improvement in τ_{SRH} caused by the GaAs interlayers is not distinguishable by the transient RA.

Fig. 6 shows the ω-2θ curve from XRD measurement. The MQW with interlayers having better crystal quality shows smaller width of fringe peaks than MQW without interlayers (Fig. 6(b)). However, despite poorer crystal quality, MQWs with larger net tensile strain give smaller peak widths, which is the opposite of what one may expect (Fig. 6(a)). This is because the XRD peak width of MQW is not determined only by the crystal quality but as well by the MQW period. The XRD peak width is inversely proportional to the period as can be confirmed from the thin fitting curve in Fig. 6 assuming perfect crystal,

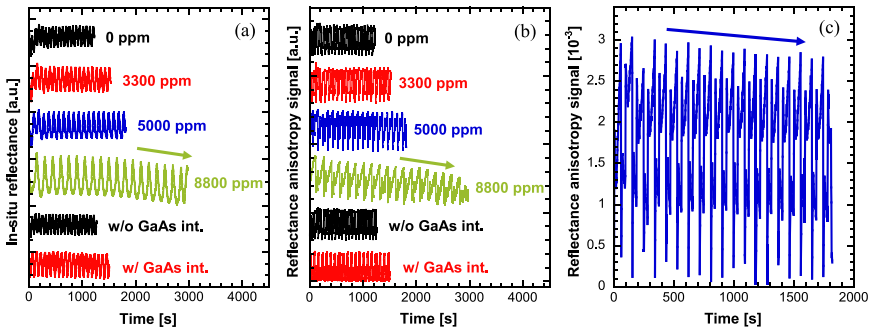

Fig. 5. In-situ measurement of transient (a) DC reflectance and (b) reflectance anisotropy at 443-nm wavelength. MQWs only for this in-situ measurement were grown 20 stacks to obtain clearer data. (c) Zoomed in reflectance anisotropy profile of the 5000-ppm-strain MQW.

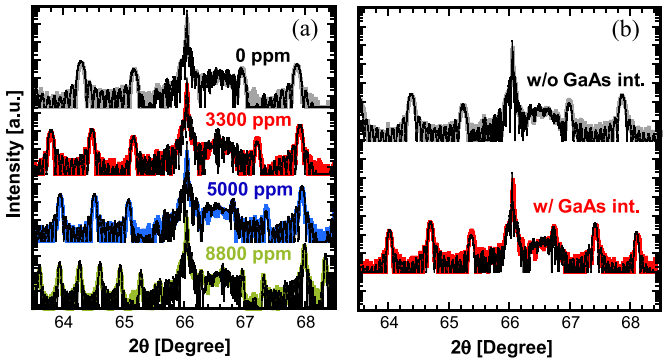

Fig. 6. ω-2θ XRD of 10-stack (a) MQWs with different net strain and (b) MQWs without and with interlayers. The thin lines are the fitting curves.

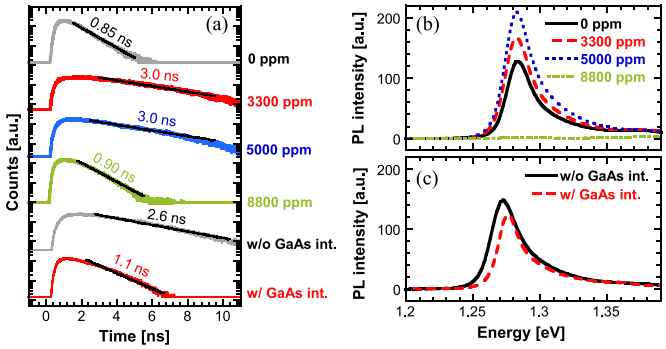

Fig. 7. (a) Time-resolved PL. The fitted decay time constants are shown with the fitted lines. Continuous-wave PL of MQW cells (b) with different net strain and (c) without and with GaAs interlayers. The excitation wavelength was 784 nm for both TRPL and CWPL measurements.

which can fit well with the measured XRD. Therefore, the comparison of XRD peak width is not the straightforward method for evaluating the quality of MQWs.

Fig. 7(a) shows the results from time-resolved PL (TRPL) measurement under the open-circuit condition, which is the standard technique for measuring carrier lifetime. The illumination wavelength was 784 nm, the pulse energy was 5.5 pJ, and the illumination area was 0.004 mm^2. TRPL interestingly shows that the luminescence decay time τ_{TRPL} is longer in MQWs with 3300- and 5000-ppm strain (both τ_{TRPL}=3.0 ns) than the strain-balanced MQW (τ_{TRPL}=0.85 ns), and becomes short again in MQW with 8800-ppm strain (τ_{TRPL}=0.90 ns).

This can be explained that the TRPL signal reflects the photogenerated carrier density inside the MQW, which decreases by both recombination process and escape process out of the MQW region, and its decay time is determined by the faster process. In the strain-balanced MQW sample, the TRPL decay time of 0.85 ns is much shorter than the SRH lifetime of 95 ns estimated from EL measurement in Fig. 4(c) and should be dominated by the escape process assisted by the internal electric field in the p-i-n junction. The escape becomes inefficient for thicker barriers due to the suppression of the tunneling transport, resulting in longer decay time in tensile-strained MQWs. The escape time eventually becomes independent of barrier thickness when barriers are so thick that carriers can only escape thermally. In the most strained MQW, the SRH lifetime becomes short enough to be observed as the decrease of the TRPL decay time; however, the TRPL decay time τ_{TRPL}=0.90 ns is still shorter than the SRH lifetime τ_{SRH}=2 ns estimated from EL measurement as some carriers can still escape out. By assuming that other processes are negligible, the estimated TRPL decay time $\tau_{TRPL} = 1/(1/\tau_{SRH} + 1/\tau_{esc})$ =1.2 ns , where the escape time τ_{esc}=3.0 ns is assumed to be the same as the 3300- and 5000-ppm samples, gives a close value to the measured decay time of 0.9 ns, supporting the above discussion.

This explanation holds for the decrease of decay time τ_{TRPL} from 2.6 ns to 1.1 ns after the interlayer insertion, which has been reported to enhance the escape of photocarriers [30]. This results in the unexpected tendency of continuous-wave PL (CWPL) intensity in Fig. 7(b)-(c) with the illumination power of 2 mW and the same illumination wavelength, showing that PL intensity drops after balancing strain and inserting interlayers. Hence, widely used TRPL and CWPL should be used with care when applied to MQW structures included in p-i-n solar cells.

The above results imply that typical evaluation techniques are not effective to detect the material quality degradation of MQWs particularly when the degradation is subtle, and that the EL technique is the suitable technique for the evaluation of MQW structures.

4. Conclusions

We introduced an electroluminescence-based evaluation technique to investigate the material quality of MQW structures embedded in p-i-n junction solar cells. Spatial defect distribution, external luminescence efficiency and SRH recombination lifetime can be obtained by analyzing the electroluminescence emission. As a demonstration, InGaAs/GaAsP MQWs with different accumulated strains and with different heterointerface designs were characterized with this technique. InGaAs/GaAsP MQWs closer to the strain-balancing condition, as expected, show improvement of the SRH lifetime. The SRH lifetime shows further improvement by a factor of 3 when GaAs interlayers are inserted between the interface of InGaAs and GaAsP, agreeing with the significant enhancement of V_{oc} by 28 mV. This technique was compared with other typical characterization methods such as in-situ DC reflectance, in-situ RA, XRD, TRPL, and CWPL. We found that most characterization techniques cannot accurately evaluate the material quality of MQWs and sometimes even give an incorrect result interpretation, implying that electroluminescence is more suitable for characterizing the quality of MQW solar cells.

Acknowledgment

A part of this study is supported by New Energy and Industrial Technology Development Organization (NEDO), Japan (P15003), and a Grant-in-Aid for JSPS Fellows (15J03447) from Japan Society for the Promotion of Science.

References

[1] A.W. Bett, S.P. Philipps, S. Essig, S. Heckelmann, R. Kellenbenz, V. Klinger, M. Niemeyer, D. Lackner, F. Dimroth, Overview about technology perspectives for high efficiency solar cells for space and terrestrial applications, Proc. 28th Eur. PV Solar Energy Conf. Exhib, pp. 1–6, 2013.
[2] M.A. Green, K. Emery, Y. Hishikawa, W. Warta, E.D. Dunlop, Solar cell efficiency tables (version 48), Prog. Photovolt. Res. Appl. 24 (2016) 905–913.
[3] A.S. Brown, M.A. Green, Detailed balance limit for the series constrained two terminal tandem solar cell, Physica E 14 (2002) 96–100.
[4] N.J. Ekins-Daukes, J.M. Barnes, K.W.J. Barnham, J.P. Connolly, M. Mazzer, J.C. Clark, R. Grey, G. Hill, M.A. Pate, J.S. Roberts, Strained and strain-balanced quantum well devices for high-efficiency tandem solar cells, Sol. Energy Mater. Sol. Cells 68 (2001) 71–87.
[5] S.M. Bedair, T. Katsuyama, P.K. Chiang, N.A. El-Masry, M. Tischler, M. Timmons, GaAsP-GaInAsSb superlattices: a new structure for electronic devices, J. Cryst. Growth 68 (1984) 477–482.
[6] K. Toprasertpong, H. Fujii, T. Thomas, M. Führer, D. Alonso-Álvarez, D.J. Farrell, K. Watanabe, Y. Okada, N.J. Ekins-Daukes, M. Sugiyama, Y. Nakano, Absorption threshold extended to 1.15 eV using InGaAs/GaAsP quantum wells for over-50%-efficient lattice-matched quad-junction solar cells, Prog. Photovolt. Res. Appl. 24 (2016) 533–542.
[7] P.-H. Wu, Y.-K. Su, I.-L. Chen, C.-H. Chiou, J.-T. Hsu, W.-R. Chen, Strain-compensated GaAsN/InGaAs superlattice structure solar cells, Jpn. J. Appl. Phys. 45 (2006) L647–L649.
[8] M. Mitsuhara, N. Watanabe, H. Yokoyama, R. Iga, N. Shigekawa, Thickness modulation and strain relaxation in strain-compensated InGaP/InGaP multiple-quantum-well structure grown by metalorganic molecular beam epitaxy on GaAs (100) substrate, J. Cryst. Growth 449 (2016) 86–91.
[9] I.E.H. Sayed, C.Z. Carlin, B.G. Hagar, P.C. Colter, S.M. Bedair, Strain-balanced

InGaAsP/GaInP multiple quantum well solar cells with a tunable bandgap (1.65–1.82 eV), IEEE J. Photovolt. 6 (2016) 997–1003.
[10] J. Hwang, J.D. Phillips, Band structure of strain-balanced GaAsBi/GaAsN superlattices on GaAs, Phys. Rev. B 83 (2011) 195327.
[11] B. Browne, J. Lacey, T. Tibbits, G. Bacchin, W. Ta-Chung, J.Q. Liu, C. Xiaodong, V. Rees, J. Tsai, J.G. Werthen, Triple-junction quantum-well solar cells in commercial production, AIP Conf. Proc. 1556 (2013) 3–5.
[12] T. Kirchartz, A. Helbig, W. Reetz, M. Reuter, J.H. Werner, U. Rau, Reciprocity between electroluminescence and quantum efficiency used for the characterization of silicon solar cells, Prog. Photovolt. Res. Appl. 17 (2009) 394–402.
[13] R. Hoheisel, F. Dimroth, A.W. Bett, S.R. Messenger, P.P. Jenkins, R.J. Walters, Electroluminescence analysis of irradiated GaInP/GaInAs/Ge space solar cells, Sol. Energy Mater. Sol. Cells 108 (2013) 235–240.
[14] L. Zhu, M. Yoshita, S. Chen, T. Nakamura, T. Mochizuki, C. Kim, M. Imaizumi, Y. Kanemitsu, H. Akiyama, Characterizations of radiation damage in multijunction solar cells focused on subcell internal luminescence quantum yields via absolute electroluminescence measurements, IEEE J. Photovolt. 6 (2016) 777–782.
[15] T. Fuyuki, H. Kondo, Y. Kaji, A. Ogane, Y. Takahashi, Analytic findings in the electroluminescence characterization of crystalline silicon solar cells, J. Appl. Phys. 101 (2007) 23711.
[16] R. Fischer, H. Morkoc, D.A. Neumann, H. Zabel, C. Choi, N. Otsuka, M. Longerbone, L.P. Erickson, Material properties of high-quality GaAs epitaxial layers grown on Si substrates, J. Appl. Phys. 60 (1986) 1640–1647.
[17] A. Delamarre, M. Paire, J.-F. Guillemoles, L. Lombez, Quantitative luminescence mapping of Cu(In, Ga)Se_2 thin-film solar cells, Prog. Photovolt. Res. Appl. 23 (2015) 1305–1312.
[18] U. Hoyer, L. Pinna, T. Swonke, R. Auer, C.J. Brabec, T. Stubhan, N. Li, Comparison of electroluminescence intensity and photocurrent of polymer based solar cells, Adv. Energy Mater. 1 (2011) 1097–1100.
[19] H. Fujii, Y. Wang, K. Watanabe, M. Sugiyama, Y. Nakano, Compensation doping in InGaAs/GaAsP multiple quantum well solar cells for efficient carrier transport and improved cell performance, J. Appl. Phys. 114 (2013) 103101.
[20] H. Sodabanlu, S. Ma, K. Watanabe, M. Sugiyama, Y. Nakano, Impact of strain accumulation on InGaAs/GaAsP multiple-quantum-well solar cells: direct correlation between in situ strain measurement and cell performances, Jpn. J. Appl. Phys. 51 (2012) 10ND16.
[21] H. Fujii, Y. Wang, K. Watanabe, M. Sugiyama, Y. Nakano, Suppressed lattice relaxation during InGaAs/GaAsP MQW growth with InGaAs and GaAs ultra-thin interlayers, J. Cryst. Growth 352 (2012) 239–244.
[22] P. Würfel, The chemical potential of radiation, J. Phys. C 15 (1982) 3967–3985.
[23] A. Delamarre, L. Lombez, J. F. Guillemoles, V. Ehrlacher, T. Lelie`vre, E. Cance`s, Investigation of solar cell properties by absolute measurement of spatially and spectrally resolved luminescence, Proc. 27th Eur. PV Solar Energy Conf. Exhib., pp. 497–499, 2012.
[24] U. Rau, Reciprocity relation between photovoltaic quantum efficiency and electroluminescent emission of solar cells, Phys. Rev. B 76 (2007) 085303.
[25] T. Mochizuki, C. Kim, M. Yoshita, J. Mitchell, Z. Lin, S. Chen, H. Takato, Y. Kanemitsu, H. Akiyama, Solar-cell radiance standard for absolute electroluminescence measurements and open-circuit voltage mapping of silicon solar modules, J. Appl. Phys. 119 (2016) 034501.
[26] T. Inoue, K. Toprasertpong, A. Delamarre, K. Watanabe, M. Paire, L. Lombez, J.-F. Guillemoles, M. Sugiyama, Y. Nakano, Quasi-Fermi level splitting evaluation based on electroluminescence analysis in multiple quantum-well solar cells for investigating cell performance under concentrated light, Proc. SPIE Phys. Simul. Photon-. Eng. Photovolt. Devices V 9743 (2016) 974316.
[27] M.A. Steiner, J.F. Geisz, I. García, D.J. Friedman, A. Duda, S.R. Kurtz, Optical enhancement of the open-circuit voltage in high quality GaAs solar cells, J. Appl. Phys. 113 (2013) 123109.
[28] K. Toprasertpong, T. Inoue, K. Watanabe, T. Kita, M. Sugiyama, Y. Nakano, Effective drift mobility approximation in multiple quantum-well solar cell, Proc. SPIE Phys., Simul., Photon-. Eng. Photovolt. Devices V 9743 (2016) 974315.
[29] J.P. Samberg, H.M. Alipour, G.K. Bradshaw, C.Z. Carlin, P.C. Colter, J.M. Lebeau, N.A. El-Masry, S.M. Bedair, Interface properties of Ga(As,P)/(In,Ga)As strained multiple quantum well structures, Appl. Phys. Lett. 103 (2013) 071605.
[30] K. Toprasertpong, N. Kasamatsu, H. Fujii, T. Kada, S. Asahi, Y. Wang, K. Watanabe, M. Sugiyama, T. Kita, Y. Nakano, Carrier time-of-flight measurement using a probe structure for direct evaluation of carrier transport in multiple quantum well solar cells, IEEE J. Photovolt. 4 (2014) 1518–1525.